REPORT DOCUMENTATION PAGE

Form Approved
OMB No. 0704-0188

Public reporting burden for this collection of information is estimated to average 1 hour per response, including the time for reviewing instructions, searching existing data sources, gathering and maintaining the data needed, and completing and reviewing this collection of information. Send comments regarding this burden estimate or any other aspect of this collection of information, including suggestions for reducing this burden to Department of Defense, Washington Headquarters Services, Directorate for Information Operations and Reports (0704-0188), 1215 Jefferson Davis Highway, Suite 1204, Arlington, VA 22202-4302. Respondents should be aware that notwithstanding any other provision of law, no person shall be subject to any penalty for failing to comply with a collection of information if it does not display a currently valid OMB control number. PLEASE DO NOT RETURN YOUR FORM TO THE ABOVE ADDRESS.

1. REPORT DATE *(DD-MM-YYYY)*
17-05-2004

REPRINT

4. TITLE AND SUBTITLE
Electromagnetic Wave Structures Within Subauroral Polarization Streams

5a. CONTRACT NUMBER

5b. GRANT NUMBER

5c. PROGRAM ELEMENT NUMBER
61102F

6. AUTHOR(S)
E.V. Mishin*, W.J. Burke, C.Y. Huang*, and F.J. Rich

5d. PROJECT NUMBER
2311

5e. TASK NUMBER
SD

5f. WORK UNIT NUMBER
A3

7. PERFORMING ORGANIZATION NAME(S) AND ADDRESS(ES)
Air Force Research Laboratory/VSBXP
29 Randolph Road
Hanscom AFB MA 01731-3010

8. PERFORMING ORGANIZATION REPORT NUMBER

20040526 044

9. SPONSORING / MONITORING AGENCY NAME(S) AND ADDRESS(ES)

11. SPONSOR/MONITOR'S REPORT NUMBER(S)
AFRL-VS-HA-TR-2004-1079

12. DISTRIBUTION / AVAILABILITY STATEMENT
Approved for Public Release; Distribution Unlimited.

*Institute for Scientific Research, Boston College, Chestnut Hill, MA

13. SUPPLEMENTARY NOTES
REPRINTED FROM: JOURNAL OF GEOPHYSICAL RESEARCH, Vol 108, No. A8, 1309, doi: 10.1029/2002JA009793, 2003.

14. ABSTRACT We report on oscillations in electronic (δE_y) and magnetic (δB_z) fields and plasma density (δN_i) observed by Defense Meteorological Satellite Program (DMSP) satellites within fast subauroral convection streams in the evening sector during the magnetic storm of 6 Nov 01. There are two types of wave phenomena. The first and more common is characterized by electromagnetic and plasma density variations that have the same frequency range of ~0.15 Hz in the spacecraft frame of reference. The second is characterized by large-amplitude plasma and field oscillations over a broader range of frequencies ~0.1 to 0.3 Hz. In this case the perturbation densities and fields appear to have different frequency responses. In this and other magnetic storms, strong waves are associated with the precipitation of ~30 keV ions. Ratios of $\delta E_y/\delta B_z$ indicate encounters with mixtures of electromagnetic (in part Alfvenic) and electrostatic modes. Poynting vectors associated with the oscillations can be directed either into or out of the ionosphere. The density perturbations appear to be extended east-west corrugations in the plasma flow stream s with north-south wavelengths of ~50 km. The δE_y and δN_i variations were anticorrelated, as required for current observations. Our analysis shows that Alfvenic perturbations are consistent with expected effects of irregular potential distribution around ionospheric density irregularities mapped to the magnetosphere. Inertial currents act to generate mesosale field-aligned currents carried by Alfven waves, as was previously discussed with regards to auroral arcs formation. We suggest that δN_i irregularities observed by DMSP satellites in the evening sector began as striated plasma patches in the polar cap that convected to subauroral latitudes.

15. SUBJECT TERMS
Ionosphere-magnetosphere interactions Plasma waves Energetic particles
Precipitating Ring current

16. SECURITY CLASSIFICATION OF:			17. LIMITATION OF ABSTRACT	18. NUMBER OF PAGES	19a. NAME OF RESPONSIBLE PERSON
a. REPORT		c. THIS PAGE			W. Burke
UNCLAS	UNCLAS	UNCLAS	SAR	11	19b. TELEPHONE NUMBER *(include area code)* 781-377-3980

AFRL-VS-HA-TR-2004-1079

JOURNAL OF GEOPHYSICAL RESEARCH, VOL. 108, NO. A8, 1309, doi:10.1029/2002JA009793, 2003

Electromagnetic wave structures within subauroral polarization streams

E. V. Mishin,[1] W. J. Burke,[2] C. Y. Huang,[1] and F. J. Rich[2]

Received 25 November 2002; revised 25 March 2003; accepted 1 May 2003; published 1 August 2003.

[1] We report on oscillations in electric (δE_Y) and magnetic (δB_Z) fields and plasma density (δN_i) observed by Defense Meteorological Satellite Program (DMSP) satellites within fast subauroral convection streams in the evening sector during the magnetic storm of 6 November 2001. There are two types of wave phenomena. The first and more common is characterized by electromagnetic and plasma density variations that have the same frequency range of ~0.15 Hz in the spacecraft frame of reference. The second is characterized by large-amplitude plasma and field oscillations over a broader range of frequencies ~0.1 to 0.3 Hz. In this case the perturbation densities and fields appear to have different frequency responses. In this and other magnetic storms, strong waves are associated with the precipitation of ~30 keV ions. Ratios of $\delta E_Y/\delta B_Z$ indicate encounters with mixtures of electromagnetic (in part Alfvénic) and electrostatic modes. Poynting vectors associated with the oscillations can be directed either into or out of the ionosphere. The density perturbations appear to be extended east-west corrugations in the plasma flow streams with north-south wavelengths of ~50 km. The δE_Y and δN_i variations were anticorrelated, as required for current conservation. Our analysis shows that Alfvénic perturbations are consistent with expected effects of irregular potential distribution around ionospheric density irregularities mapped to the magnetosphere. Inertial currents act to generate mesoscale field-aligned currents carried by Alfvén waves, as was previously discussed with regards to auroral arcs formation. We suggest that δN_i irregularities observed by DMSP satellites in the evening sector began as striated plasma patches in the polar cap that convected to subauroral latitudes. *INDEX TERMS:* 2431 Ionosphere: Ionosphere/magnetosphere interactions (2736); 2439 Ionosphere: Ionospheric irregularities; 2471 Ionosphere: Plasma waves and instabilities; 2716 Magnetospheric Physics: Energetic particles, precipitating; 2778 Magnetospheric Physics: Ring current

Citation: Mishin, E. V., W. J. Burke, C. Y. Huang, and F. J. Rich, Electromagnetic wave structures within subauroral polarization streams, *J. Geophys. Res.*, *108*(A8), 1309, doi:10.1029/2002JA009793, 2003.

1. Introduction

[2] Subauroral magnetic field lines map to the inner magnetosphere earthward of the electron plasma sheet. During intensifications of geomagnetic activity, electric fields permeate the inner magnetosphere with widespread consequences for the global distributions of plasmas, particles, and fields. The domain of auroral particle precipitation in the ionosphere expands equatorward. In large numbers, ring current (RC) ions enter previously forbidden parts of the plasmasphere. The source of the ions can be either substorm injections or large convection fields associated with magnetic storms. Ultimately, plasma pressure grows in the inner magnetosphere. In regions where gradients in plasma pressure become misaligned with gradients in the magnetic flux tub volume, field-aligned currents (FACs) flow to couple the magnetosphere with the conjugate ionosphere [*Vasyliunas*, 1970]. The recently developed kinetic transport models of *Fok et al.* [2001] and *Liemohn et al.* [2001] indicate that the azimuthal pressure gradient and radial flux tube volume gradient are largely responsible for the region 2 FACs. FACs affect the distributions of electric potential required to satisfy current continuity in the ionosphere. Via field-line mapping, potential in the inner magnetosphere is redistributed. Altered potential distributions are usually described in terms of partial shielding of the convection electric field by the ring current [e.g., *Southwood and Wolf*, 1978; *Harel et al.*, 1981; *Spiro et al.*, 1981; *Senior and Blanc*, 1984; *Erickson et al.*, 1991; *Peymirat and Fontaine*, 1994].

[3] Owing to the low conductivity of the nightside ionosphere at subauroral latitudes, channels of intense, poleward directed electric fields develop to produce enhanced (>500 m/s) streams of westward convection. This phenomenon is described by the names polarization jets (PJ) [*Galperin et al.*, 1974] or subauroral ion drifts (SAID) [*Spiro et al.*, 1979; *Anderson et al.*, 1993, 2001]. *Yeh et al.* [1991] and *Burke et al.* [1998, 2000] pointed out that

[1]Institute for Scientific Research, Boston College, Chestnut Hill, Massachusetts, USA.

[2]Air Force Research Laboratory, Hanscom Air Force Base, Massachusetts, USA.

Copyright 2003 by the American Geophysical Union.
0148-0227/03/2002JA009793$09.00

latitudinal extents of westward drifting plasma at subauroral latitudes during periods of high activity may be much greater than the 1° to 2° typical of SAID/PJ structures. Recently, *Foster and Burke* [2002] suggested the name subauroral Polarization Streams (SAPS) to include plasma flow events that have both broad and narrow extents in latitude.

[4] Previous experimental and modeling efforts treated SAPS electric fields as varying smoothly across the structure. However, observations from Defense Meteorological Satellite Program (DMSP) satellites and Millstone Hill radar [*Erickson et al.*, 2002] often indicate the presence of irregular substructures with scale size of order tens km within SAPS. While *Maynard et al.* [1980] mentioned that storm time electric fields adjacent to the plasmapause were strongly variable, consequences of their observations were not pursued. On the other hand, it is known that short-scale density irregularities in the *F* region can significantly modify radio wave propagation. For example, the HAARP HF heating facility (see, e.g., [*Pedersen and Carlson*, 2001] or http://www.haarp.alaska.edu) is located at normally subauroral latitudes. The presence of plasma irregularities in the overhead ionosphere can affect the structure of the heated region.

[5] Plasma irregularities of sufficient scale size can affect the dynamics of warm plasmas in the conjugate magnetosphere and ionosphere [*Ogawa and Sato*, 1971]. This subject has been addressed in numerous studies of magnetosphere-ionosphere coupling at auroral latitudes [*Atkinson*, 1971; *Maltsev et al.*, 1977; *Miura and Sato*, 1980]. To the degree that plasma density irregularities represent conductance irregularities, polarization electric fields and field-aligned currents must develop to maintain current continuity across the irregularities. Modeling by *Miura and Sato* [1980] shows that consequently altered potential patterns create feedback conditions inducing structured auroral electron precipitation that enhances the regions of initially high ionospheric conductance. Data presented here mostly come from subauroral latitudes where no measurable electron precipitation was present. We suggest that an analogous electromagnetic feedback develops, in this case between ionospheric irregularities and conjugate ring current ions.

[6] The purpose of this report is to extend understanding of irregularity structures found within SAPS structures. This is accomplished through analyses of perturbations in local plasma densities and drifts as well as magnetic fields observed by sensors on the DMSP F15 satellite during the magnetic storm of 6 November 2001. The following section describes the relevant sensor suite on DMSP F15. The observation section has three parts. A brief description of the magnetic storm provides a context for understanding DMSP measurements. A detailed exposition of measurements acquired during one of the SAPS crossing illustrates the quasi-dc circuit and embedded small-scale plasma and fields irregularities. Our analysis demonstrates that the irregularities often have narrow frequency spectra. Both quasi-electrostatic and electromagnetic wave structures can coexist in close physical proximity. At times the Poynting flux carried by the electromagnetic waves was directed away from the ionosphere. Characteristics of the full set of DMSP measurements are summarized in tabular form. The final section discusses possible wave-generation mechanisms and the roles of ring current, plasmasphere, and ionosphere.

2. Instrumentation

[7] DMSP satellites are three-axis stabilized spacecrafts that fly in circular, sun-synchronous polar (inclination 98.7°) orbits at an altitude of ~840 km. The geographic local times of the orbits are either near the 1800–0600 (F13) or 2100–0900 (F12, 14, 15) meridians. Owing to the offset between the geographic and geomagnetic poles DMSP satellites sample wide range of magnetic local times (MLT) over the course of a day. The ascending nodes of DMSP orbits are on the duskside of the Earth. Thus the satellites move toward the northwest in the evening LT sector. Each satellite carries a suite of sensors to measure (1) fluxes of auroral particles (SSJ4), (2) the densities, temperatures, and drift motions of ionospheric ions and electrons (SSIES), and (3) perturbations of the Earth magnetic field (SSM).

[8] Identical SSJ4 sensors are mounted on the top sides of DMSP satellites to measure fluxes of precipitating electrons and ions in the energy range between 30 eV and 30 keV [*Hardy et al.*, 1984]. The measurements are made by four detectors, one high energy detector and one low energy detector for the each of the particle types. The ion detectors have no mass discrimination capabilities. Each detector has 10 logarithmically spaced energy steps. The high energy detectors step from 30 keV to 1 keV and the low energy detectors step from 1 keV to 30 eV. The last step of the high energy detector is set at the same energy as the first step of the low energy detector. Only particles within an energy band of approximately 10% of the channel step energy freely pass from aperture to the channeltron detector. The particle fluxes are measured within a solid angle of 2° × 5° for the high energy channels and 4° × 5° for the low energy channels centered on local vertical. Each detector has a dwell time of 0.098 s and a 0.002 s period between steps to stabilize the voltage. Each detector make a complete 10 step sequence in 1 s. One 20 point ion and one 20 point electron is returned once per second. Actually, the spectra have only 19 points because of the redundancy of the 1 keV energy step. Unfortunately, fluxes of ions with energies below 1 keV are unavailable from the F15 satellite as the low-energy ion detector failed.

[9] SSIES sensors are mounted on the ram facing surfaces of the satellites. They consist of (1) an ion drift meter to measure the horizontal (V_H) and vertical (V_V) cross-track components of plasma drift within the range of ±3000 m/s and a one-bit resolution of 12 m/s for ambient ion densities greater than $5 \cdot 10^3$ cm^{-3}; (2) retarding potential analyzer to measure ion temperatures (T_i), composition, and the in-track component of plasma drift ($V_\parallel$); (3) an ion trap to measure the total ion density (N_i); and (4) a spherical Langmuir probe mounted on an 80-cm boom to measure the density (N_e) and temperature (T_e) of ambient electrons [*Rich and Hairston*, 1984]. The drift measurements are made at a time resolution of 1/6 s and the density measurements are at 24 Hz.

[10] SSM sensors are triaxial fluxgate magnetometers that are mounted on the bodies of the F12–F14 spacecrafts. For DMSP flight F15 the magnetometers are mounted on 5-m

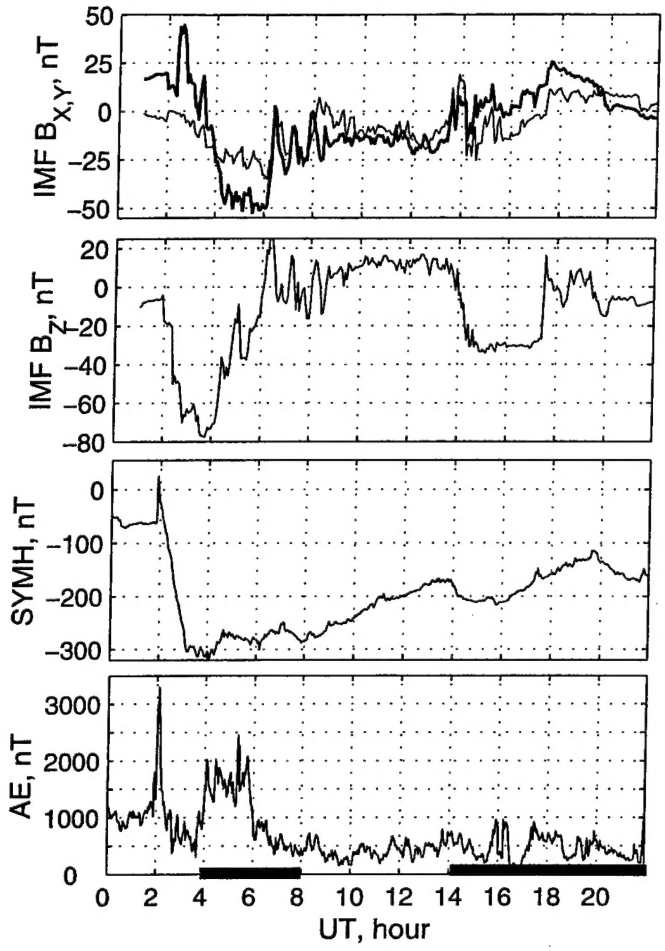

Figure 1. (top) IMF B_Y (heavy line), B_X (light line), and B_Z. (bottom) SYMH and AE indices; bold lines designate the intervals where SAPS were observed.

booms. These sensors are much less susceptible to spacecraft-generated electromagnetic contamination than their body-mounted predecessors. The high-precision magnetic field measurements required for the present study all come from the F15 satellite. Magnetic field components are sampled at a rate of 12 (Y and Z) and 10 (X) s^{-1} and are presented in a satellite-centered coordinate system. The X axis points in the downward direction. The Y axis points along the spacecraft velocity. The Z axis completes a right-hand coordinate system. Positive Z components generally point in the antisunward direction. Data are presented as differences ($\Delta\mathbf{B}$) between measured values and those assigned by the IGRF-90 magnetic field model ($\mathbf{B_0}$). Nearly simultaneous observations from the SSM, SSIES, and SSJ4 sensors on the other spacecrafts are used to interpret F15 measurements.

3. Observations

[11] Salient features of the 6 November 2001 magnetic storm are summarized in Figure 1. The top two plots respectively show the GSM Y, X, and Z components of the interplanetary magnetic field (IMF) as measured at the ACE satellite near the first Lagrangian point (L_1). For comparison with Earth-based measurements, ACE data were shifted by one 1 to allow for propagation from L_1. At the time of this writing, solar wind data for most of the day are unavailable. We note, however, that between the beginning and end of the day the solar wind speed rose from ~430 to ~730 km/s and the density decreased from ~10 to ~2 cm^{-3}. The bottom two plots respectively show the SYMH [*KYOTO*] and AE indices. Information provided by the SYMH index is similar to Dst but is presented at a cadence of 1-min versus 1-hour averages.

[12] Data in Figure 1 show that between 0150 and 0153 UT SYMH and AE increased from −62 to 25 and ~1000 to ~3300 nT, respectively, then rapidly decreased to ~ −300 and ~500 nT. Shortly after 0300 UT SYMH remained near −300 nT before beginning to recover 1 hour and 20 min later, likely, following a northward turning of the IMF B_Z. At the same time AE sharply increased to ~2000 nT until ~0545 UT. The SYMH recovery proceeded smoothly to ~−170 nT at 1400 UT when SYMH again decreased to ~−215 nT for about 2 hours. The main-phase decrease in SYMH corresponds to a southward turning of the IMF B_Z that reached consistent values near −70 nT. The second southward turning of the IMF B_Z to about −30 nT between 1400 and 1600 UT corresponds to the second SYMH intensification. During this period AE experienced ±200 nT variations until about 1540 UT when it increased up to ~1000 nT, then decreased and increased again at about 1730 UT. Finally, attention is directed to two bold horizontal lines extending from about 0400 to 0800 and 1400 to 2300 UT. They delineate intervals during the recovery phase when F15 crossed SAPS structures (16 events).

[13] Figure 2 provides an example typical of SAPS structure crossed by DMSP. It was sampled during a Northern Hemisphere pass in the evening sector in the storm's recovery phase. The top two panels show directional differential number fluxes of downcoming electrons and ions, respectively. The trace in the third panel gives 1-s averages of the horizontal component of the cross-track drift velocity (V_H) measured by the drift meter in meters per second. The light and heavy traces in the bottom panel give 1-s averages of ΔB_Y and ΔB_Z, respectively. Data are plotted as functions of UT and MLat. Magnetic local time (2118 MLT) practically did not change. By definition, the SAPS' poleward boundary coincides with the equatorward boundary of auroral electron precipitation (the dashed line) and was crossed at ~1802:50 UT. The maximum plasma velocity of 1.75 km/s was sampled at ~1802:30 UT (~52° MLat). Irregular structures appear in V_H and magnetic field traces.

[14] Figure 3 provides the in-track (Y) component of the electric field E_Y[mV/m] = $10^{-6}V_H$[m/s] · B_{0X}[nT], the cross-track component of the magnetic field ΔB_Z, and ion density N_i. At northern latitudes, positive slopes in the ΔB_Z trace correspond to field-aligned currents into the ionosphere. Apparently, the maximum electric field roughly coincides with the deepest depletion in the N_i trace. All three quantities contain small-scale irregularities superposed on the main trends of the E_Y, ΔB_Z, and N_i traces. It is worth mentioning that an examination of the high-resolution raw data (not shown) does not change our results. We consider first dc then ac aspects of these observations.

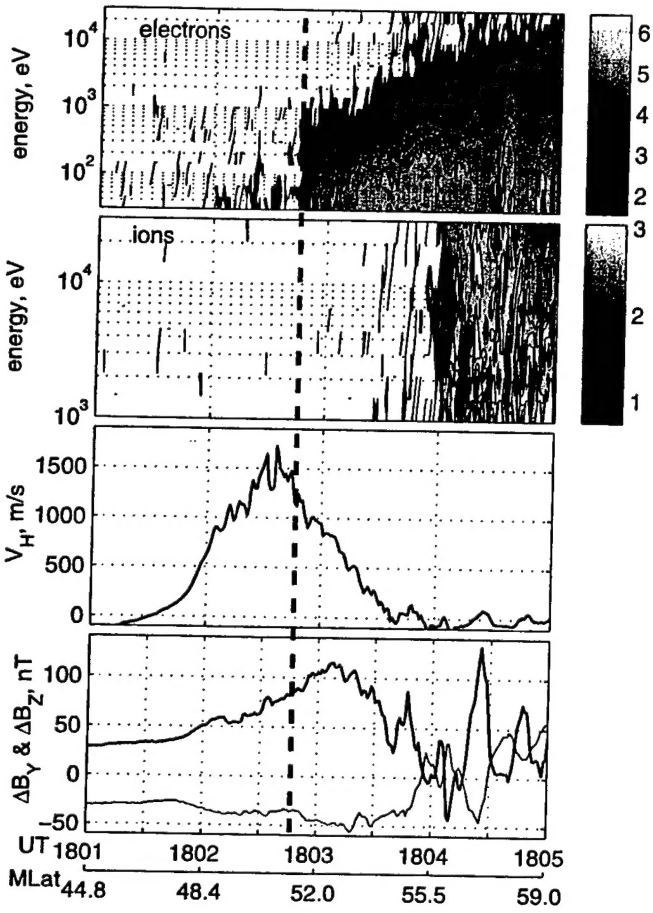

Figure 2. Top and second panels show electron and ion energy-time spectrograms (logarithmic scale); 1, 2,... on the color bar stand for 10^1, 10^2... $1/(cm^2 \cdot s \cdot ster \cdot eV)$. Third panel shows horizontal component of the convection velocity across the satellite trajectory in meters per second. Bottom panel shows deviation of measured Y(light line) and Z (heavy line) components of magnetic field from IGRF values. The dashed line indicates the SAPS' poleward boundary.

[15] A simple application of Ampere's law and the current continuity equation, using the infinite current sheet approximation gives

$$\hat{j}_{\parallel} = \frac{1}{\mu_0} \frac{\partial \widehat{\Delta B_Z}}{\partial Y \cos\alpha} = \nabla \cdot \hat{\mathbf{I}}_{\perp}. \qquad (1)$$

Here μ_0 is the permeability of free space, $\mathbf{I}_{\perp} \simeq \boldsymbol{\Sigma}_P \Delta \mathbf{E}$ is the height-integrated ionospheric current perpendicular to $\mathbf{B}_0$, and Σ_P is the height-integrated Pederson conductivity (in the nightside subauroral ionosphere Hall conductance Σ_H is negligible). Herein, $\hat{\Psi}$ designates spatially-averaged ("dc") perturbations obtained through the application of lowpass ($\Delta t > 20$ s) filter to Ψ; $j_{\parallel}$, ΔB, E, and Σ_P are expressed in $\mu A/m^2$, nT, mV/m, and siemens, respectively.

[16] For a satellite traveling poleward at a speed of 7.5 km/s, equation (1) is approximated by

$$\hat{j}_{\parallel} \approx 0.1 \frac{\partial}{\partial t} \widehat{\Delta B_Z}. \qquad (2)$$

In the interval between 1802 and 1803 UT $\widehat{\Delta B_Z}$ increased by about 50 nT, indicating that $\hat{j}_{\parallel}$ was about 0.1%μ A/m2. Simultaneous variations in ΔB_Z and ΔB_Y (Figure 2) support our adoption of the infinite current sheet approximation [*Fung and Hoffman*, 1992]. Combining equation (1) and Ohm's law, *Smiddy et al.* [1980] obtained $\partial_Y\left(\widehat{\Delta B_Z} - \mu_0 \widehat{\Sigma_P}\widehat{\Sigma_Y}\right) = 0$, which reduces to

$$\widehat{\Delta B_Z} - 1.256 \cdot \widehat{\Sigma_P} \cdot \widehat{E_Y} = \text{const} \qquad (3)$$

Equation (3) indicates that variations in $\widehat{\Delta B_Z}$ and $\widehat{E_Y}$ should track each other in regions of constant $\widehat{\Sigma_P}$. From 1802:10 to 1802:35 UT $\widehat{E_Y}$ and $\widehat{\Delta B_Z}$ increased by ~35 mV/m and ~35 nT, respectively. During this interval the cross correlation coefficient between $\widehat{E_Y}$ and $\widehat{\Delta B_Z}$ was ≃0.98. Over this interval, one can estimate $\widehat{\Sigma_P}$ as ~0.8 mhos. Between 1802:40 and 1803:10 the slopes of the $\widehat{\Delta B_Z}$ and $\widehat{E_Y}$ traces have opposite signs due to $\widehat{\Sigma_P}$ increase to ~1.4 mhos. At the center of the high-flow channel, where $E_{max} \approx 55$ mV/m, the rate of column Joule heating is $\widehat{\Sigma_P} E^2_{max} \approx 2$ mW/m^2. An integration of equation (1) along the spacecraft trajectory shows that the total perturbation is proportional to $J_{\parallel} = \int j_{\parallel} ds \approx 0.6$ A/m.

[17] Figure 4 shows perturbation quantities designated δE_Y, δB_Z, and δN_i obtained through the application of bandpass elliptic filter ($0.05 \leq f \leq 0.45$ Hz) to the E_Y, ΔB_Z, and N_i measurements, respectively. Spectral analyses of the δE_Y, δB_Z, and δN_i measurements are shown in the

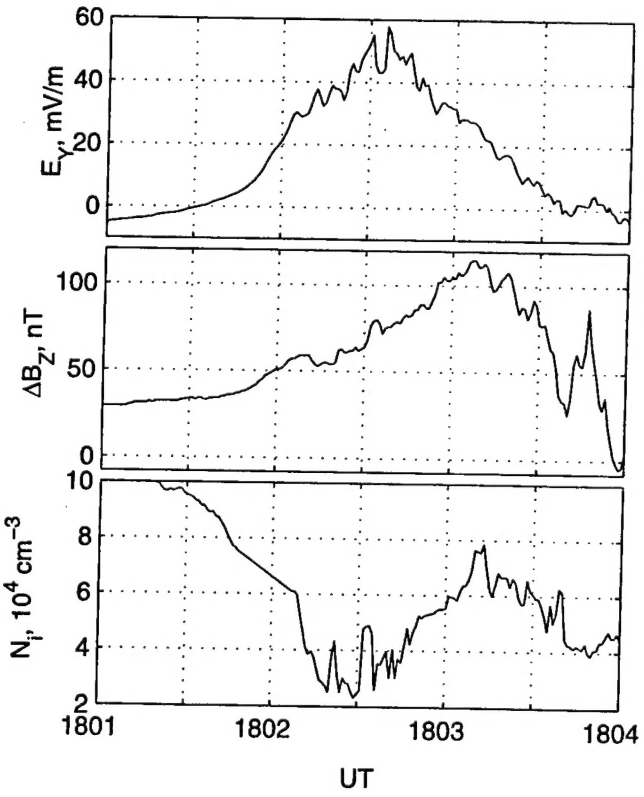

Figure 3. Variations of the poleward convection electric field (top), deviation of the eastward component of the geomagnetic field from IGRF (middle), and ion density (bottom).

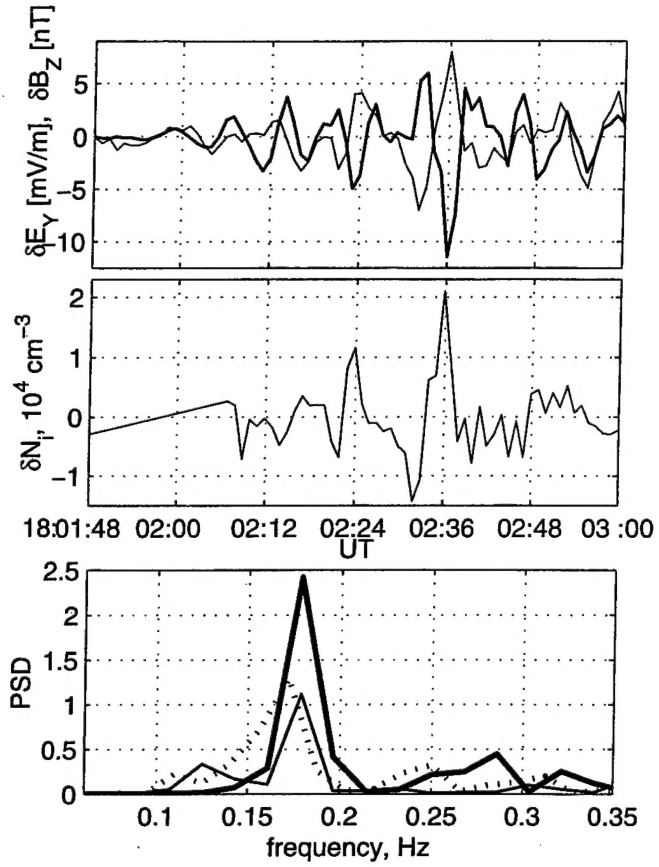

Figure 4. (top) Oscillations of the electric (heavy line) and magnetic (light line) fields. (middle) Ion density oscillations. (bottom) Power spectral density of the electric field (heavy line), magnetic field (light line), and ion density (dotted line) oscillations.

bottom panel. The largest spectral component for the electric and magnetic field variations is at ~0.17 Hz. The δN_i spectral peak is at ~0.165 Hz.

[18] Using measured values of N_i and B_0 we have calculated the local Alfvén speed $V_A = B_0/\sqrt{\mu_0 M N_i}$ where M is the ion mass. Current voltage sweeps of the retarding potential analyzer on F15 indicate that O^+ was the dominant ion species. Within the low density region of the SAPS structure $V_A \approx$ 1300 km/s. In the top panel of Figure 5 we compare calculated values of V_A with those of "phase velocities" $V_{ph} = |\delta E_Y/\delta B_Z|$. In regions where $V_{ph}/V_A \approx 1$, associated waves are almost purely electromagnetic (likely Alfvén waves). Significant deviation from unity indicates the presence of a strong electrostatic component (note that points with $V_{ph}/V_A \geq 10$ were excluded).

[19] Finally, the bottom panel of Figure 5 gives calculated values of the field-aligned component of Poynting flux $S_X = \delta E_Y \delta B_Z/\mu_0$ (in $\mu W/m^2$) carried by electromagnetic waves. Positive (negative) values indicate that wave-energy flows into (out of) the ionosphere. Apparently, in the region of highest plasma flow near the center of the structure, wave-energy flows away from the ionosphere at a maximum rate of ~75 $\mu W/m^2$. It is noteworthy that δB_Y was less than $0.15 \cdot \delta B_Z$ during this period.

[20] An examination of the figures yields the following four observations:

[21] 1. During a ~50-s period after ~1802:10 UT the three traces show very similar fluctuations.

[22] 2. The E_Y and N_i variations are anticorrelated over the interval.

[23] 3. Prior to 1802:20 the phase difference between δE_Y and δB_Z vary from ~0° to ~90°, while after ~1802:42 UT δE_Y and δB_Z vary in phase with each other. During the intervening period they are ≈180° out of phase.

[24] 4. The field-aligned component of Poynting flux S_X is directed into (out of) the ionosphere where the variations are in (out of) phase.

[25] We have surveyed measurements of V_H and N_i on DMSP F12, F13, and F14, taken in the evening sector within ±30 min of the SAPS crossing by F15 shown in Figure 2. In each instance we found signatures of the SAPS structure with the maximum westward flow speed near 52° MLat, extending for at least 3 hours in local time. Anticorrelated irregularity structures appeared in the V_H and N_i traces. Spectral analysis of these data showed narrow peaks near ~0.17 Hz. Electromagnetic interference from spacecraft contaminates the body-mounted magnetometers on F12–F14 and render estimates of Poynting fluxes unreliable.

[26] Table 1 lists the universal times (UT), magnetic latitude (MLat), and magnetic local times (MLT) at which maximum westward plasma velocities (V_{max}) were observed by F15 within 16 SAPS structures. Also listed in Table 1 are the corresponding maximum electric fields (E_{max}), the frequency of irregularities (f), and the field-aligned component of Poynting flux (S_X) deduced from electric and magnetic field irregularities within SAPS.

[27] One can see that electromagnetic substructures observed by F15 within SAPS events were detected in two parts of the storm's recovery phase (Figure 1). The first group (0400–0800 UT) occurred in the early recovery phase near the deepest excursion of SYMH and the second rise of AE after the first northward turning of the IMF B_Z. They were located ~3°–5° equatorward in magnetic latitude of

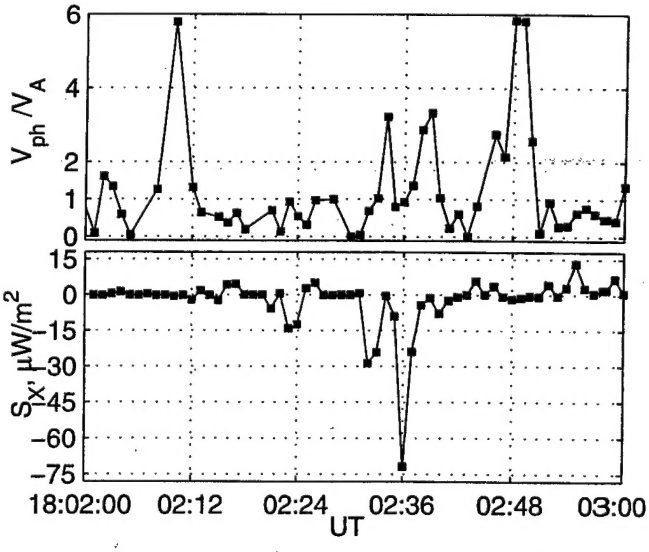

Figure 5. (top) V_{ph}/V_A-ratio. (bottom) Poynting flux in $\mu W/m^2$.

Table 1. SAPS and Wave Structures From DMSP F15, 6 November 2001

UT	MLat	MLT	V_{max}, km/s	E_{max}, mV/m	f, Hz	S_X(μW)/m^2
0356	−46°	22.8	1.7	35	0.2	+1/−2.5
0423	46°	20.7	1.5	45	0.15&0.35	+1200/−500
0539	−47°	22.7	0.55	10		
0752	50°	20.5	1.45	50	0.16	+10/−15
1412	−53°	22.3	0.8	30	0.17	+1.8/−0.4
1439	54°	21.0	0.5	15		
1554	−50°	21.8	1.4	45	0.12	+100/−20
1621	51°	21.0	1.9	60	0.19	+1/−2
1736	−52°	21.3	0.7	20		
1803	**52°**	**21.3**	**1.75**	**55**	**0.17**	**−75**
1915	−53°	21.4	1.0	25		
1944	52°	21.4	1.2	40	0.18	+3/−0.5
2057	−52°	21.4	0.8	20		
2125	52°	21.4	1.1	35	0.19	+0.5/−0.75
2237	−52°	21.5	1.8	45	0.2	+0.75/−1
2307	52°	21.9	1.75	55	0.15	+13/−5

the second (1400–2400 UT) group. Five cases with no entries in the last two columns had irregularity amplitudes too small to be measured by DMSP sensors. These were associated with values of $V_{max} < 1$ km/s. However, in one case with $V_{max} = 0.8$ km/s irregularities were detected. In cases with detectable irregularities the dominant frequencies were confined to a fairly narrow band, 0.18 ± 0.03.

[28] The final column of Table 1 lists the field-aligned Poynting fluxes in μW/m^2 calculated using simultaneous measurements of δB_Z and δE_Y. We adopt a convention using positive (negative) values of S_X to indicate net flows of electromagnetic energy into (out of) the ionosphere. The range of S_X covers more than three orders of magnitude. Almost half of the SAPS events with detectable irregularities had energy flows >10 μW/m^2, associated with $E_{max} \geq$ 45 mV/m. Thus the example presented above is typical of the discussed phenomena.

[29] The obvious exception is the SAPS event encountered near 0423 UT in which the peak to peak variability of V_H oscillations exceeded dc plasma velocities and the downward Poynting flux reached 1.2 mW/m^2. Figure 6 shows particle fluxes as well as the measured electric and magnetic fields and ion density. The vertical dashed line marks the low-latitude boundary of auroral electron precipitation. Attention is directed to three features of the data. First, significant fluxes of precipitating 30 keV ions were detected between 0423:20 and 0423:30 UT, equatorward of the auroral boundary. These fluxes probably represent the low-energy portion of the ring-current distribution function [*Smith and Hoffman*, 1974]. Second, V_H modulations appear to change at ~04:23:30 UT. Finally, the background plasma density decreased from 2 10^5 cm^{-3} at 0422:00 to a minimum of ~5 10^4 cm^{-3} near 0423:00 UT then recovered at 0424:30 UT. Densities sampled between 0423:00 and 0424:00 UT were marked by irregularities similar to those found in Figure 3. The average Alfvén speed in the trough decreased from about 900 to 700 km/s between 0423:00 and 0424:00 UT.

[30] Figure 7 displays spectral analyses of δN_i, δB_Z, and δE_Y measurements taken between 0423:00 and 0424:00 UT. For simplicity we divide the interval up into half-minute intervals before (Figure 7a) and after (Figure 7b) 0423:30 UT. Prior to 0423:30 UT both δB_Z, and δE_Y had strong spectral peaks near 0.15 Hz. While δN_i oscillations occurred near 0.15 Hz, the bulk of its spectral power was in the 0.22 to 0.26 Hz band. After 0423:30 UT the spectral range of δB_Z and δN_i variations broadened. δE_Y spectral power decreased near 0.15 Hz but increased dramatically at 0.35 Hz. The overall effect of data presented in Figure 7 suggests that plasma and field fluctuations observed prior to 0423:30 UT are similar to those observed during the other SAPs events (cf. Figure 4). Variability observed after this time were of a considerably more complex nature.

[31] As with the SAPS event near 1800 UT (Figure 5) we have compared "phase velocities" obtained from the ratios

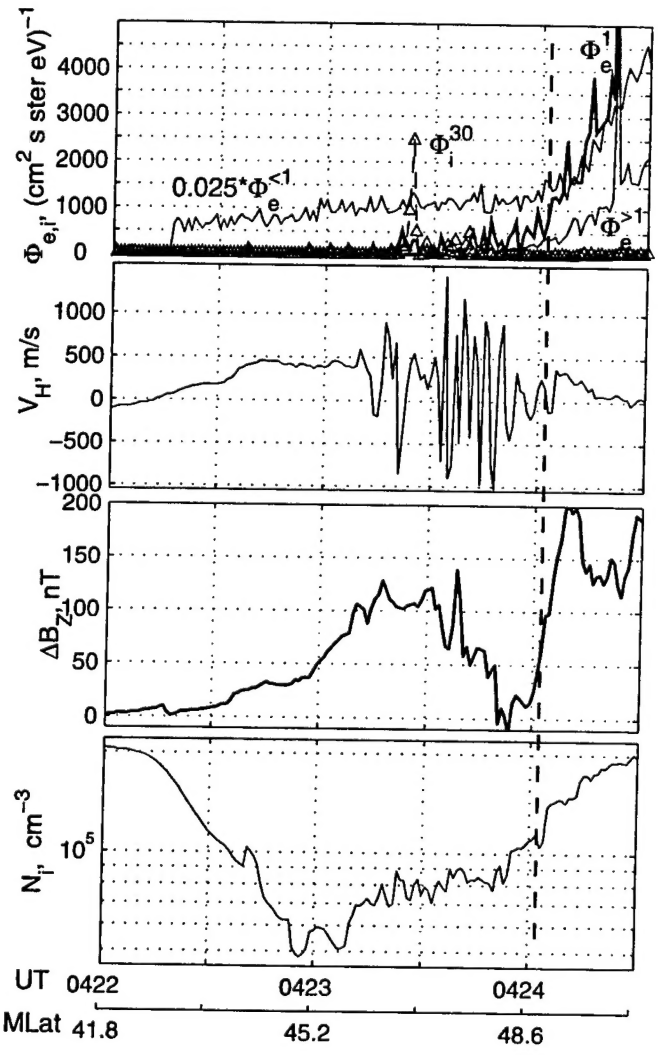

Figure 6. Top panel shows electron and ion differential number fluxes $\Phi_{e,i}$ in (cm^2 · s · ster · eV)$^{-1}$. Φ_e^1 (heavy line) and Φ_i^{30} (triangles) are the fluxes of 1 keV electrons and 30 keV ions, respectively. $\Phi_e^{>1}$ and $\Phi_e^{<1}$ stand for the averaged electron fluxes in the channels 11 to 19 (>1 keV) and 1 to 9 (<1 keV), respectively. Second panel shows horizontal component of the convection velocity across the satellite trajectory in meters per second. Third panel shows the deviation of the Z component of the geomagnetic field from IGRF. Bottom panel shows the ion density variation. The dashed line indicates the plasma sheet equatorward boundary.

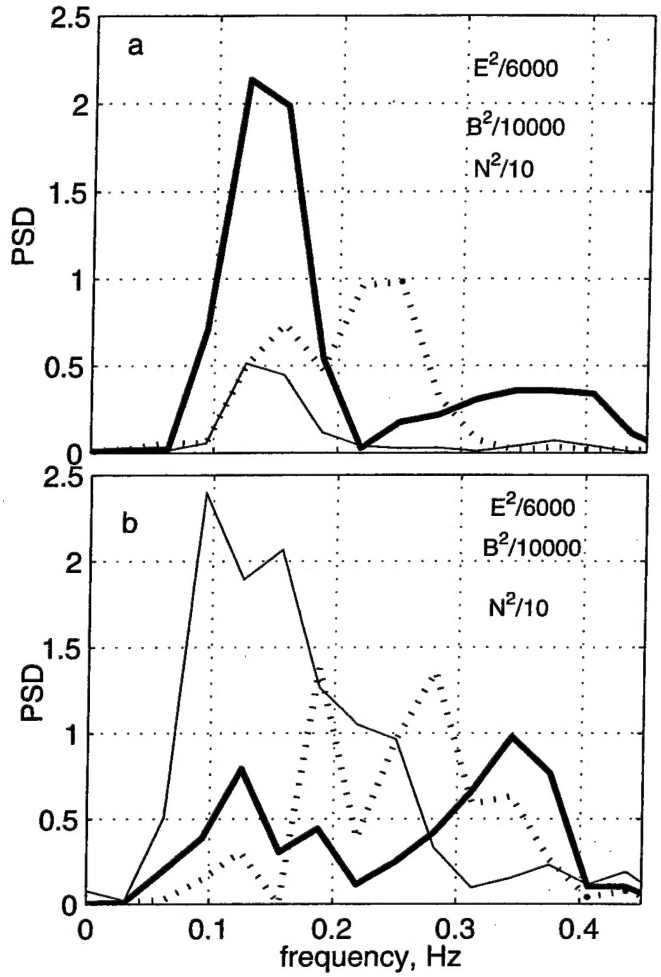

Figure 7. Power spectral densities of δN_i (dots), δB_Z (light lines), and δE_Y (heavy lines) (a) before and (b) after 0423:30 UT.

of δE_Y and δB_Z with Alfvén velocities computed from measured values of N_i and B_0. These comparisons show that in significant portions of the 0423 to 0424 UT interval the perturbation were Alvénic. DMSP measurements suggest that intense electric field events associated with SAPS structures are highly localized and/or short lived. They were not encountered while crossing the conjugate SAPS structure at 0356 UT. No large amplitude δE_Y perturbations were detected by F12–F14 in SAPS structures crossed within a half hour of 0423 UT. The event however is not unique. We have observed similar δE_Y oscillations during other magnetic storms on the poleward side of SAPS structures. Like the event shown in Figure 6, they too were associated with the precipitation energetic ions just equatorward of the auroral electron boundary.

4. Discussion

[32] The previous section provides two detailed examples of wave-like variations in plasma density as well as magnetic and electric fields, observed by DMSP F15 while crossing midlatitude troughs during the magnetic storm of 6 November 2001. In both cases, relatively weak field-aligned currents into the ionosphere are associated with intense poleward electric fields that drive westward plasma convection within the troughs. Data summarized in Table 1 indicate that these wave-like perturbations are stable features in storm time midlatitude troughs and are found in the conjugate ionospheres. Comparisons of $\delta E_Y/\delta B_Z$ ratios with local Alfvén speeds indicate that both electrostatic and electromagnetic variations were sampled. Similar FACs, electric fields, and density troughs were detected by F14 and F13 near 2000 and 1800 LT, respectively. δN_i and δE_Y variations had spectral characteristics similar to those observed at the local time of F15.

[33] The wave-like perturbations appear consistently in the evening MLT sector just equatorward of the auroral electron precipitation boundary. Within this region DMSP detected weak field-aligned currents into the ionosphere, strong poleward electric fields, and deep troughs in the local ionospheric plasma density. Low values of Σ_P inferred from the ratio of quasi dc magnetic to electric field variations suggest that the troughs extend in altitude to the peak of the F layer. The absence of sunlight and measurable fluxes of auroral particles indicate that the E layer contains little to no plasma.

[34] We distinguish between two manifestations of wave phenomena. The first and more common appears in spectra accumulated during the intervals 1802:00 to 1803:00 UT (Figure 4) and 0423:00 to 0423:30 UT (Figure 7a). They are characterized by electromagnetic and plasma density variations that have the same frequency range of 0.1 to 0.2 Hz. The second and more dramatic manifestation of wave-like perturbations was sampled in the 30 s after 0423:30 UT and was characterized by large-amplitude plasma and field oscillations over a broader range of frequencies extending across the 0.2 to 0.3 Hz range. In the second case the perturbation densities and fields appear to have different frequency responses. In this and other magnetic storms strong waves are associated with the precipitation of energetic ions.

[35] The remainder of this discussion considers several possible causal mechanisms for interpreting the first type of the wave phenomena. It is necessary to examine the nature of the electromagnetic fluctuations. We show that the data are consistent with a complex coupling between the ionosphere and magnetosphere consequent to the formation of deep troughs associated with SAPS structures. We also suggest that the source of the density irregularities was located far to the east of the DMSP trajectory.

4.1. Cavity-Mode Interpretation

[36] It is tempting to suggest that DMSP observations of δB_Z, δE_Y, and δN_i variations with similar frequencies across high-speed convection channels in the trough indicate the presence of resonant shear Alfvén waves in a cavity. This interpretation is consistent with observing similar variability in the conjugate ionospheres. By comparing the ratio $\delta E_Y/\delta B$ with the local Alfvén speed we established that the observed waves have both electromagnetic and electrostatic components. The electromagnetic (EM) part propagates along magnetic field lines. The field-aligned component of the wave vector $k_{||} = 2\pi f_{EM}/V_A$ varies with the magnetic field and plasma density along individual magnetic field lines. We view the electrostatic (ES) variations as zero-frequency

spatial structures with wave lengths $\lambda_{ES} = V_{sat}/f_{ES}$. For V_{sat} = 7.5 km/s and f_{ES} = 0.15 Hz, λ_{ES} = 50 km and $k_Y \approx 0.13$ km^{-1}.

[37] Data presented in Figure 3 indicate that the plasma and field oscillations occurred between 1802:00 and 1803:00 UT. During this interval DMSP F15 moved from 48.4° to 52° in magnetic latitude. In a magnetic dipole approximation, this corresponds to L = 2.27 and 2.56, respectively, where $L = 1/\cos^2\Lambda$ is the McIlwain parameter and Λ is the invariant latitude. It is easily shown that the length of dipole field lines between two conjugate ionospheric points is $D(\Lambda) = 2LR_E \int_0^\Lambda d\zeta \cos\zeta\sqrt{1+3\sin^2\zeta}$, where ζ is the magnetic latitude and $R_E \simeq 6380$ km. Performing the integration gives $D(48.4°)$ = 26730 km and $D(52°)$ = 32350 km. To satisfy the resonance condition, $D(\Lambda)$ must be equal to an integral number of half wavelengths between the conjugate ionospheres. If these distances represent a full wavelength, then with f_{EM} = 0.16 Hz, the average Alfvén speed between the conjugate ionospheres is $V_A(48.4°)$ = 4275 and $V_A(52°)$ = 5180 km/s. These are significantly higher than Alfvén speeds calculated from plasma densities and magnetic fields measured by DMSP in the topside ionosphere or inferred for conjugate plasmaspheric parameters [e.g., *Chappell*, 1972]. Thus we conclude that the observed wave phenomena cannot result from a simple cavity-mode resonance of a ~0.15 Hz wave.

4.2. Ring-Current Source Interpretation

[38] *Kennell and Petschek* [1966] demonstrated that whenever the fluxes of energetic particles trapped in the inner magnetosphere exceed certain threshold limits, the amplitudes of background electromagnetic waves grow, causing the gyroresonant particles to diffuse toward the atmospheric loss cone. Whistlers and Alfvén waves are responsible for the pitch-angle diffusion of energetic electrons and protons, respectively. The presence of field-aligned currents across the region of interest indicates the presence of energetic ring current ions at conjugate locations in the magnetosphere [*Vasyliunas*, 1970]. The resonance condition is

$$2\pi f - k_\parallel v_\parallel = 2\pi f^+ \qquad (4)$$

where $v_\parallel$ and $k_\parallel$ are field-aligned components of velocity and wave vector, respectively, and f^+ is the local ion gyrofrequency. The most prolonged interactions occur near the magnetic equator where the plasma density and magnetic field strength change most slowly. In the magnetic dipole approximation, at L = 2 near the magnetic equator $B_{eq} \approx 3800$ nT. Energetic ring current ions, however, may be H^+ or O^+. Their cyclotron frequencies in a 3800 nT magnetic field are 57 and 3.6 Hz, respectively. As for a 0.16 Hz wave $f \ll f^+$, equation (4) can only be satisfied if the wave and energetic ion travel in opposite directions. The dispersion relation for Alfvén waves is $k_\parallel = 2\pi f/V_A$. The local Alfvén speed is determined by the local magnetic field and the density of cold plasmaspheric ions. Typical plasmaspheric densities near L = 2 are $n_c \sim 5 \cdot 10^9$ m^{-3} and are mostly H^+ ions [*Chappell*, 1972]. Substitution into equation (4) shows that the energy of resonant ions E_R is

$$E_R = \frac{1}{2}Mv_\parallel^2 \simeq \frac{B_{eq}^2}{2\mu_0 n}\frac{M}{M_H}\left(\frac{f^+}{f}\right)^2 \qquad (5)$$

Here M and M_H represent the masses of ring-current ions and plasmaspheric hydrogen ions, respectively. Substituting gyrofrequencies into equation (5) shows that the energy of resonant ring-current ions, independent of species, must be $\gg$1 MeV. This greatly exceeds the several tens of keV measured ion energies of storm time ring current ions near their earthward boundary [*Smith and Hoffman*, 1974]. Thus we conclude that ring-current particles cannot be the direct sources of the Alfvén waves characteristic of the first type wave phenomena (Figure 2). This conclusion is consistent with the observation that DMSP did not detect fluxes of precipitating 1–33 keV ions during such events. At $L \approx 2.5$ precipitating particles should have equatorial pitch angles <12°. At the location of DMSP the local dip angle is about 67°, and the atmospheric loss cone has a width of about 58°. The vertically looking SSJ4 detector intercepts ions with pitch angles of 23° ± 2.5°, well within the local loss cone.

[39] It is worth noting that *Iyemori and Hayashi* [1989] and *Erlandson et al.* [1993] observed down-going electromagnetic waves with ~0.1–1 Hz frequencies (Pc1 range) at $L \geq 4$ in the dusk and morning sectors. *Erlandson et al.* [1993] suggested that those are electromagnetic ion cyclotron (EMIC) waves generated by RC protons in the RC-plasmasphere overlap region. Could this mechanism contribute to formation of the down-going Poynting flux and energetic ion precipitations in the dusk-evening sector (Figure 6)? *Denton et al.* [1992] have shown that the frequency of the most unstable EMIC waves varies as $B_{eq}^{1.4}/n_c^{0.2}$. Given $B_{eq}(L) \sim L^{-3}$, one can expect at $L \sim 2$ the frequency of order several Hz for H^+ and ~0.3 Hz for O^+. Therefore O^+-driven EMIC waves within the RC-plasmasphere interaction region cannot be ruled out as a possible contributor to the second type wave phenomena (Figure 6 after 0423:30 UT).

4.3. Magnetosphere-Ionosphere Coupling Interpretation

[40] Striations of relatively high and low plasma density in the nightside trough mark the regions of correspondingly higher and lower height-integrated Pedersen conductivity. To maintain current continuity, polarization electric fields must develop to enhance/diminish E_Y in regions of negative/positive plasma density variations. We have already noted that as expected variations in δE_Y anticorrelated with those of δN_i. Altered potential distributions near δN_i variations must then map to the magnetosphere. The role of Alfvén waves in transferring this information to the magnetosphere has been discussed by a number of investigators who model auroral arcs as latitudinally narrow strips of enhanced ionospheric conductivity [e.g., *Ogawa and Sato*, 1971; *Maltsev et al.*, 1977]. In its proper frame of reference, equatorward convecting plasma experiences time varying electric fields $(\mathbf{V_Y}\cdot\nabla)\mathbf{E_Y}$. Consequent field-aligned currents are carried by Alfvén waves that distribute space charge $(\nabla \cdot \delta E_Y)/\mu_0 V_A$ along magnetic field lines to turn them into the appropriate new equipotentials [e.g., *Kan and Sun*, 1985]. These models predict that as rapidly developing δN_i structures alter potential patterns, electromagnetic energy in the form of upward moving Poynting flux should be observed above the ionosphere. Consistent with this prediction, DMSP detected episodes of upward wave Poynting flux while crossing the SAPS structure.

[41] *Miura and Sato* [1980] pointed out that the transmission of electromagnetic energy from the ionosphere to the magnetosphere cannot be the only interaction. Rather, a feedback develops whereby the magnetosphere also affects the ionosphere. Altered potential distributions in the magnetosphere affect the drift velocities of the energetic particle populations that in their proper reference frames see time-varying electric fields. The consequent inertial drifts carry currents $\mathbf{j}_\perp = (MN_i e/B^2)d\delta\mathbf{E}/dt$. In regions where the energetic particles experience $d\delta\mathbf{E}/dt < 0$, the conditions for an MHD generator $\mathbf{j}_\perp \cdot \delta\mathbf{E} < 0$ are satisfied. That is such regions extract mechanical energy from the particles to launch Alfvén waves carrying field-aligned current and Poynting flux toward the ionosphere. Qualitatively this adaptation of the *Miura and Sato* [1980] scenario coincides with the DMSP observations.

4.4. Source for Observed Plasma Irregularities

[42] The DMSP measurements should be considered on two spatial scales sizes. The larger scale size is the ~4.5° latitudinal width of the SAPS structure and the smaller one is that of the plasma irregularity structures. The coincidental formation of plasma density troughs and SAPS structures was predicted based on theoretical considerations by *Schunk et al.* [1976] and *Banks and Yasuhara* [1978]. They argued that intense electric fields in the subauroral ionosphere would lead to the formation of deep troughs through a combination of plasma outflow and enhanced recombination stemming from the charge exchange reaction $O^+ + N_2 \rightarrow NO^+ + N$ whose rate k_{N_2} increases in the convecting/heated plasma. Actually, *Schunk et al.* [1976] made use of the relation $k_{N_2} \sim T_i^2 \sim [\mathbf{E} \times \mathbf{B_0}]^4$. *Anderson et al.* [1991] have argued that the plasma outflow related to frictional ion heating is the main cause of the formation of the deep troughs. *Moffett et al.* [1998] reported enhancements of the ion and electron temperatures ~4000 and 6000 K within the SAPS-related troughs. It is known that k_{N_2} increases with the level of vibrational excitation of N_2 (see the latest assessment of the laboratory measurements by *Viggiano and Williams* [2001]). As the vibrational population of N_2 rises with T_e, electron heating may significantly contribute to the trough formation [e.g., *Moffett et al.*, 1998; *Pavlov et al.*, 2000].

[43] Importantly, no significant (>100 m/s) plasma outflows were detected within the density troughs under study. On the other hand, significant variations of the ion and electron temperature were observed (Figure 8). Note that the time resolution of T_e was 4 (top panel) and 32 s (bottom), while T_i was sampled at a rate of 0.25 s^{-1}. One can see that the electron temperature achieved maximum 9200 and 6500 K, respectively, at the density minimum. Just the opposite, T_i decreased to ~1000 K at the center. The electron energy flux of $Q_T \sim (1-3)10^{10}$ eVcm^{-2}s^{-1} from the ring current-plasmasphere interaction region [e.g., *Moffett et al.*, 1998] can explain the electron temperature variation $T_e \propto Q_T/N_i$. In turn, the ion temperature decrease in the center can be understood in terms of frictional heating, provided the plasma density in the heating region decreases stronger than E^{-2}.

[44] Why nearly monochromatic density irregularities with wavelengths of several tens of km should form is beyond the scope of this observational report. The likely

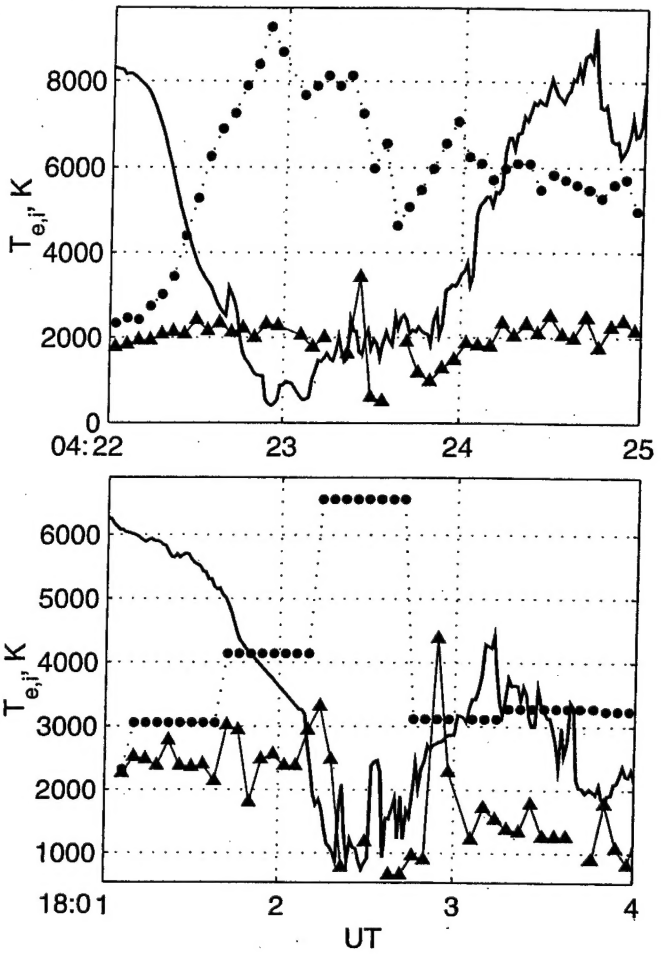

Figure 8. Variations of the electron (dots) and ion (triangles) temperature within the (top) 0423 UT and (bottom) 1803 UT SAPS; solid line shows the (scaled-down) ion density.

source, the drift instability, requires the $\mathbf{E} \times \mathbf{B}$ drift to have a component in the same direction as the plasma density gradient [e.g., *Ossakow and Chaturvedi*, 1979]. It implies a weak (tangential) westward (eastward) component of the electric field at subauroral latitudes that renders the equatorward (poleward) wall of the trough drift-unstable. To the contrary, the most intense irregularities were colocated with the fastest average sunward flows in the middle of the trough. One can speculate that the reduction of the plasma density due to electron heating and vice versa may serve as a generation mechanism of the density irregularities. Indeed, the relations $\delta N_i \sim -\delta T_e^a$ with $a > 0$ and $T_e \propto Q_T/N_i$ provide positive feedback in the system. However, a mechanism that defines the scale size of the thermal perturbations has yet to be found.

[45] We suggest that the irregularities observed by DMSP between 1802:00 and 1802:50 UT were not created locally. With these observations in mind, it is useful to ask where cold plasmas sampled by DMSP F15 between 1801:20 and 1802:50 were located 1 hour prior to observation. To answer this question, it is necessary to recall that the corotational motion of the plasma was subtracted from SSIES measurements shown in Figure 2. At the a latitude of 50° the

corotation speed is about 0.38 km/s. Cold plasma detected before (after) 1801:50 UT reached DMSP F15 from earlier (later) local times to the west (east) of its trajectory. In a corotating frame of reference plasma associated with the largest amplitude irregularities moved westward about 1.12 km/s. Assuming that the plasma velocity was nearly constant, at 1702:00 UT the irregularities were about 4000 km to the east. At 50° latitude one hour in local time corresponds to an east-west separation of ~1300 km. Thus 1 hour prior to detection the plasma element would be located ~3 hours to the east, that is, in the midnight sector.

[46] Empirical models of plasma convection show that plasma streamlines (equipotentials) exit the polar cap cross the auroral oval with substantial alignments in the north-south direction. In the auroral oval, streamlines develop larger east-west alignments. Some streamlines continue toward the dayside through the auroral oval while other pass to subauroral latitudes. Near 1800 UT, DMSP F13 (near 1800 MLT) and F15 (near 2100 MLT), respectively, measured potential drops of about −80 and −70 kV across the afternoon convection cell. At both locations the potential drop across the SAPS was ~−25 kV. *Burke et al.* [1998] showed that during magnetic storms the potential drops at subauroral latitudes are significant fractions of the total potential in the afternoon cell. The equipotentials that reach subauroral latitudes cross the polar cap near the separatrix between the afternoon and morning convection cells. These considerations suggest the following scenario:

[47] 1. Enhanced magnetic merging at the magnetopause captures finite volumes of dayside plasma then convects them as "plasma patches" into and across the polar cap [*Kelley and Vickrey*, 1984].

[48] 2. Within the polar cap the trailing edge of the patches are drift unstable yielding alternating regions of relatively high and low density at *F* layer altitudes [*Tsunoda*, 1988; *Crowley*, 1996]. Significantly, *Kivanç and Heelis* [1997] reported DE 2 observations of fully structured patches.

[49] 3. After convecting across the polar cap the striated topside plasma enters the nightside auroral oval where the plasma density is augmented at *E* region altitudes due to auroral precipitation. The main effect of the *E* region is to enhance transport processes in the *F* region, shorting out polarization electric fields [e.g., *Farley*, 1959], suppressing the drift instability, thus freezing existing large-scale striations in place and eliminating small scales.

[50] 4. Plasma drifting along equipotentials near the separatrix between the dusk and dawn cells convects to subauroral latitudes where it becomes entrained within a SAPS structure in the midnight sector. In the absence of sustaining auroral electron precipitation, *E* layer plasma quickly recombines and disappears. Within the SAPS, deep troughs are formed at *F* layer altitudes. In the process the striations that developed in the polar cap are maintained as alternating streams of high and low plasma density. However, since the directions of convection and density gradients have become nearly perpendicular, no further drift-mode growth occurs.

[51] 5. As indicated in the subsection on M-I coupling, the regions of alternating high and low electric field are the sites of generation of Alfvén waves carrying field-aligned currents to the magnetosphere and to the conjugate ionosphere.

[52] It is easy to test the hypothesis that the plasma and field striations observed by F15 within the SAPS originated in the polar cap. We have examined plasma densities measured by DMSP F13 and F15 in the polar cap near the times listed in Table 1. During periods when striations were detected in the midlatitude trough we also found structured plasma in the polar cap. Densities within the structures were $\sim(2.5 \pm 1) \cdot 10^5$ cm^{-3}. If our conjecture is correct the plasma density at 840 km must have decreased by a factor of 10 in convecting from ~85° MLat in the midnight sector of the polar cap to ~52° MLat, 2100 MLT in the subauroral ionosphere.

5. Conclusion

[53] Oscillations in electric and magnetic fields and plasma density were observed by DMSP satellites in the evening sector at subauroral latitudes during the 6 November 2001 magnetic storm. Those were detected within fast convection streams near the deepest depletions of the midlatitude trough. The latter coincide with the electron temperature enhancements ≥6000 K. We distinguish between two manifestations of wave phenomena. The first and more common is characterized by electromagnetic and plasma density variations within the same frequency range of ~0.15 Hz in the spacecraft frame of reference. The second type is characterized by large amplitude plasma and field oscillations over a broader range of frequencies ~0.2 to 0.3 Hz. The perturbation densities and fields appear to have different frequency responses. In this and other magnetic storms, strong waves are associated with the precipitation of ~30 keV ions.

[54] The observed waves comprise electromagnetic (in part Alfvénic) and electrostatic modes. Electromagnetic energy fluxes can be directed both into and out of the ionosphere. The density perturbations appear to be extended east-west corrugations in the plasma flow streams with north-south wavelengths of ~50 km. The δE_Y and δN_i variations were anticorrelated, as required for current conservation. Alfvénic perturbations are consistent with expected effects of irregular potential distribution around ionospheric density irregularities mapped to the magnetosphere. Inertial currents act to generate mesoscale field-aligned currents carried by Alfvén waves, as was previously discussed with regards to auroral arcs formation. On the other hand, O^+ -driven EMIC waves within the RC-plasmasphere interaction region cannot be ruled out as a possible contributor to the second type wave phenomena. We suggest that δN_i irregularities observed by DMSP satellites in the evening sector began as striated plasma patches in the polar cap that convect to subauroral latitudes.

[55] **Acknowledgments.** Authors thank John Foster and Anatoly Streltsov for valuable comments. This research was supported in part by the HF Active Auroral Research Program (HAARP) under AFRL contract F19628-02-C-0012 with Boston College and by Air Force Office of Scientific Research. Data from the ACE satellite were obtained through the NASA/GSFC website. AE and SYMH indices were obtained through the website of the World Data Center for Geomagnetism, Kyoto.

[56] Arthur Richmond thanks Phillip Anderson and Robert E. Erlandson for their assistance in evaluating this paper.

References

Anderson, P., R. Heelis, and W. Hanson, The ionospheric signatures of rapid subauroral ion drifts, *J. Geophys. Res.*, *96*, 5785, 1991.

Anderson, P., W. Hanson, R. Hellis, J. Graven, D. Baker, and L. Frank, A proposed production model of rapid subauroral ion drifts and their relationship to substorm evolution, *J. Geophys. Res.*, *98*, 6069, 1993.

Anderson, P., D. Carpenter, K. Tsuruda, T. Mukai, and F. Rich, Multisatellite observations of rapid subauroral ion drifts (SAID), *J. Geophys. Res.*, *106*, 29,585, 2001.

Banks, P. M., and F. Yasuhara, Electric fields and conductivity in the nighttime E region: A new magnetosphere-ionosphere-atmosphere coupling effect, *Geophys. Res. Lett.*, *5*, 1047, 1978.

Burke, W., et al., Electrodynamics of the inner magnetosphere observed in the dusk sector by CRRES and DMSP during the magnetic storm of June 4–6, 1991, *J. Geophys. Res.*, *103*, 29,399, 1998.

Burke, W., A. Rubin, N. Maynard, L. Gentile, P. Sultan, F. Rich, O. de la Beaujardiere, C. Huang, and G. Wilson, Ionospheric disturbances observed by DMSP at mid to low latitude during magnetic storm of June 4–6, 1991, *J. Geophys. Res.*, *105*, 18,391, 2000.

Chappell, C. R., Recent satellite measurements of the morphology and dynamics of the plasmasphere, *Rev. Geophys.*, *10*, 951, 1972.

Crowley, G., Critical review of ionospheric patches and blobs, in *Review of Radio Science, 1993–1996*, pp. 619–648, Oxford Univ. Press, New York, 1996.

Denton, R., M. Hudson, and I. Roth, Loss-cone-driven ion cyclotron waves in the magnetosphere, *J. Geophys. Res.*, *97*, 12,093, 1992.

Erickson, G., R. Spiro, and R. Wolf, The physics of the Harang discontinuity, *J. Geophys. Res.*, *96*, 1633, 1991.

Erickson, P. J., J. C. Foster, and J. M. Holt, Inferred electric field variability in the polarization jet from Millstone Hill E region coherent scatter observations, *Radio Sci.*, *37*(2), 1027, doi:10.1029/2000RS002531, 2002.

Erlandson, R., T. Aggson, W. Hogey, and J. Slavin, Simultaneous observations of subauroral electron temperature enhancements and electromagnetic ion cyclotron waves, *Geophys. Res. Lett.*, *20*, 1723, 1993.

Farley, D. T., A theory of electrostatic fields in a horizontally stratified ionosphere subject to a vertical magnetic field, *J. Geophys. Res.*, *64*, 1225, 1959.

Fok, M.-C., R. Wolf, R. Spiro, and T. Moore, Comprehensive computational model of Earth's ring current, *J. Geophys. Res.*, *106*, 8417, 2001.

Fung, S., and R. A. Hoffman, Finite geometry effects of field-aligned currents, *J. Geophys. Res.*, *97*, 8569, 1992.

Galperin, Y., Y. Ponomarev, and A. Zosimova, Plasma convection in the polar ionosphere, *Ann. Geophys.*, *30*, 1, 1974.

Hardy, D. A., L. K. Schmidt, M. S. Gussenhoven, F. J. Marshall, H. C. Yeh, T. L. Shumaker, A. Huber, and J. Pantazis, Precipitating electron and ion detectors (SSJ/4) for block 5D/Flights 4–10 DMSP satellites: Calibration and data presentation, *Tech. Rep. AFGL-TR-84-0317*, Air Force Geophys. Lab., Hanscom Air Force Base, Mass., 1984.

Harel, M., R. Wolf, P. Reiff, R. Spiro, W. Burke, F. Rich, and M. Smiddy, Quantitative simulation of a magnetospheric substorm: 1. Model logic and overview, *J. Geophys. Res.*, *86*, 2217, 1981.

Iyemori, T., and K. Hayashi, PC 1 micropulsations observed by MAGSAT in the ionospheric F region, *J. Geophys. Res.*, *94*, 93, 1989.

Kan, J. R., and W. Sun, Simulation of the westward traveling surge and Pi2 pulsations during substorms, *J. Geophys. Res.*, *90*, 10,911, 1985.

Kelley, M. C., and J. F. Vickrey, F region ionospheric structure associated with anisunward flow near the dayside cusp, *Geophys. Res. Lett.*, *11*, 907, 1984.

Kennell, C. F., and H. E. Petschek, Limit on stably trapped particle fluxes, *J. Geophys. Res.*, *71*, 1, 1966.

Kivanç, Ö., and R. A. Heelis, Structures in ionospheric number density and velocity associated with polar cap ionization patches, *J. Geophys. Res.*, *102*, 307, 1997.

Liemohn, M., J. Kozyra, M. Thomsen, J. Roeder, G. Lu, J. Borovsky, and T. Cayton, Dominant role of the asymmetric ring current in producing the storm time Dst*, *J. Geophys. Res.*, *106*, 10,883, 2001.

Maltsev, Y., W. Lyatsky, and A. Lyatskaya, Currents over the auroral arcs, *Planet. Space Sci.*, *25*, 53, 1977.

Maynard, N., T. Aggson, and J. Heppner, Magnetospheric observation of large subauroral electric fields, *Geophys. Res. Lett.*, *7*, 881, 1980.

Miura, A., and T. Sato, Numerical simulation of global formation of auroral arcs, *J. Geophys. Res.*, *85*, 73, 1980.

Moffett, R., A. Ennis, G. Bailey, R. Heelis, and L. Brace, Electron temperatures during rapid subauroral ion drift events, *Ann. Geophys.*, *16*, 450, 1998.

Ogawa, T., and T. Sato, New mechanism of auroral arcs, *Planet. Sp. Sci.*, *19*, 1393, 1971.

Ossakow, S. L., and P. K. Chaturvedi, Current convective instability in the diffuse aurora, *Geophys. Res. Lett.*, *6*, 332, 1979.

Pavlov, A., T. Abe, and K.-I. Oyama, Comparison of the measured and modeled electron densities and temperatures in the ionosphere and plasmasphere during 20–30 January 1993, *Ann. Geophys.*, *18*, 1257, 2000.

Pedersen, T., and H. C. Carlson, First observations of HF heater-produced airglow at the High Frequency Active Auroral Research Program facility: Thermal excitation and spatial structuring, *Radio Sci.*, *36*, 1013, 2001.

Peymirat, C., and D. Fontaine, Numerical simulation of magnetospheric convection including effect of field-aligned currents and electron precipitation, *J. Geophys. Res.*, *99*, 11,155, 1994.

Rich, F. J., and M. Hairston, Large-scale convection patterns observed by DMSP, *J. Geophys. Res.*, *79*, 3827, 1984.

Schunk, R., P. Banks, and W. Raitt, Effect of electric fields and other processes upon on the nighttime high-latitude F layer, *J. Geophys. Res.*, *81*, 3271, 1976.

Senior, C., and M. Blanc, On the control of magnetospheric convection by the spatial distribution of ionospheric conductivities, *J. Geophys. Res.*, *89*, 261, 1984.

Smiddy, M., W. J. Burke, M. C. Kelley, N. A. Saflekos, M. S. Gussenhoven, D. A. Hardy, and F. J. Rich, Effects of high-latitude conductivity on observed convection electric fields and Birkeland currents, *J. Geophys. Res.*, *85*, 6811, 1980.

Smith, P. H., and R. A. Hoffman, Direct observations in the dusk hours of the characteristics of storm time ring current particles during the beginning of magnetic storms, *J. Geophys. Res.*, *79*, 964, 1974.

Southwood, D., and R. Wolf, An assessment of the role of precipitation in magnetospheric convection, *J. Geophys. Res.*, *83*, 5227, 1978.

Spiro, R., R. Heelis, and W. Hanson, Rapid subauroral ion drifts observed by Atmospheric Explorer C, *Geophys. Res. Lett.*, *6*, 657, 1979.

Spiro, R., M. Harel, R. Wolf, and P. Reiff, Quantitative simulation of a magnetospheric substorm: 3. Plasmaspheric electric fields and evolution of the plasmapause, *J. Geophys. Res.*, *86*, 2261, 1981.

Tsunoda, R. T., F region irregularities: A review and synthesis, *Rev. Geophys.*, *26*, 719, 1988.

Vasyliunas, V., Mathematical models of magnetospheric convection and its coupling to the ionosphere, in *Particles and Fields in the Magnetosphere*, edited by B. M. McCormac, p. 60, D. Reidel, Norwell, Mass., 1970.

Viggiano, A., and S. Williams, Ion-molecule kinetics at high temperatures (300–1800 K): Derivation of internal energy dependencies, *Adv. Gas-Phase Ion Chem.*, *4*, 85, 2001.

Yeh, H.-C., J. Foster, F. Rich, and W. Swider, Storm time electric field penetration observed at mid-latitude, *J. Geophys. Res.*, *96*, 5707, 1991.

W. J. Burke and F. J. Rich, AFRL/VSBX, 29 Randolph Road, Hanscom Field, MA 01731, USA. (William.Burke@hanscom.af.mil; Frederick.Rich@hanscom.af.mil)

C. Y. Huang and E. V. Mishin, Institute for Scientific Research, Boston College, 402 St. Clements Hall, 140 Commonwealth Avenue, Chestnut Hill, MA 02467-3862, USA. (Cheryl.Huang@hanscom.af.mil; Evgenii.Mishin@hanscom.af.mil)